Evidence of a robust universality class in the critical behavior of self-propelled agents: Metric versus topological interactions

Lucas Barberis[1] and Ezequiel V. Albano[1,2]

[1]*Instituto de Física de Líquidos y Sistemas Biológicos, CONICET, UNLP, Calle 59, Nr. 789 (1900) La Plata, Argentina*
[2]*Departamento de Física, Facultad de Ciencias Exactas, UNLP, La Plata, Argentina*

The nature of the interactions among self-propelled agents (SPA), i.e., topological versus metric or a combination of both types, is a relevant open question in the field of self-organization phenomena. We studied the critical behavior of a Vicsek-like system of SPA given by a group of agents moving at constant speed and interacting among themselves under the action of a topological rule: each agent aligns itself with the average direction of its seven nearest neighbors, independent of the distance, under the influence of some noise. Based on both stationary and dynamic measurements, we provide strong evidence that both types of interactions are manifestations of the same phenomenon, which defines a robust universality class. Also, the cluster size distribution evaluated at the critical point shows a power-law behavior, and the exponent corresponding to the topological model is in excellent agreement with that of the metric one, further reinforcing our claim. Furthermore, we found that with topological interactions the average distance of influence between agents undergoes large fluctuations that diverge at the critical noise, thus providing clues about a mechanism that could be implemented by the agents to change their moving strategy.

I. INTRODUCTION

The study of self-propelled agent (SPA) systems has attracted great interest from the physical community [1–3] and has stimulated huge theoretical and experimental activity (for recent reviews see, e.g., [4,5]). Also, modeling swarming and flocking contributes to the understanding of natural phenomena and becomes relevant for many practical and technological applications, e.g., collective robotic motion, design and control of artificial microswimmers, and many other self-propelled particle systems.

The seminal model developed by Vicsek *et al.* in 1995 [1] has become a fruitful paradigm for studying self-organization phenomena. It considers N agents moving in a two-dimensional space at constant speed v_0. These agents choose their trajectories by trying to align their moving direction with the average direction of *all* agents inside a circle with a unitary radius with a perturbation due to a uniform noise. Thus the system reaches an ordered sate for a low enough noise below some critical value η_c and undergoes a phase transition into a disordered state beyond η_c [1,3–6]. Mathematical and statistical models of SPA attempt to describe a wide range of complex phenomena in biological systems, from bacteria [7,8] and cells [9] at the microscopic scale to swarms of insects [10] and flocks of birds [11] at larger scales. Particularly, careful measurements of huge flocks of starlings have given a new clue to understanding how organisms can self-organize. In fact, Cavagna *et al.* [12] have determined that each bird of the flock follows a fixed number of individuals, seven in the case of starlings [13]. So the way those birds choose their neighbors to decide their direction of motion is of topological nature, in contrast to the metric rule of the Vicsek model [1] used in most simulations [2–6]. Since the discovery of that feature, several studies [11,14–16] have been performed in order to understand topological interactions. However, the influence of both types of interactions acting at a local level at the onset of ordering at

macroscopic scales is still an open question that merits careful study.

Within this wide context, the goal of this paper is to present and discuss extensive simulation results aimed at understanding both the dynamic and stationary critical behaviors of a topological Vicsek-like system of SPA. For this purpose, we organized the paper as follows: Section II provides the definition of the model and details of the numerical method used. Our results are presented and discussed in Sec. III, while the conclusions are stated in Sec. IV.

II. TECHNICAL ASPECTS OF THE NUMERICAL SIMULATIONS

The simulations are performed in such a way that the results can be compared to those presented previously in [17] for the metric model. Thus, the density is set at $\rho = 0.1$ for four choices of the number of agents ($4096 \leqslant N \leqslant 32\,768$), and we also set $v_0 = 0.1$, so that the system is in a low-density and low-velocity regime. Measurements within the stationary regime are performed after disregarding 10^5 time steps until the system leaves the transient regime from a uniformly random initial state. Also, two kinds of dynamic simulations are performed at criticality: (a) relaxation dynamic measurements such that the system is released from an ordered state and (b) short-time dynamic measurements performed by releasing the system from disordered states. All dynamic measurements are averaged over 500 different realizations. We evaluate the standard order parameter defined as $\phi \equiv \frac{1}{Nv_0}|\sum_{i=1}^{N}\vec{v}_i|$, as well as its high-order moments and the cumulant. The velocity vectors $\vec{v}_i$ have constant speed v_0, and their directions θ_i fluctuate according to

$$\theta_i^{t+1} = \langle\theta^t\rangle_{k_{nn}} + \eta\pi\xi + \alpha. \tag{1}$$

Then, each agent i takes a new direction θ_i^{t+1}, given by the average over the actual directions of its k_{nn} nearest neighbors,

with the addition of a uniform noise in the range $[-\pi, \pi]$ generated by a random variable ξ. The amplitude η regulates the intensity of the perturbations and is the control parameter. The last term (α) is an extra rotation of the same small random angle imposed on all particles at each time step in order to avoid the artifacts mentioned in [4–6,18,19]. Also, the kinematics of the system is updated by

$$\vec{r}_i^{\,t+1} = \vec{r}_i^{\,t} + \vec{v}_i^{\,t} \Delta t; \quad \Delta t = 1, \qquad (2)$$

where $\vec{r}_i$ are the positions of the agents.

III. RESULTS AND DISCUSSION

We found that the ability of the system to reach an ordered state is more robust against noise when k_{nn} is increased. In fact, the model adopts a mean-field behavior for $k_{nn} > 18$, while ordered states are almost absent for $k_{nn} \leqslant 2$. So, arbitrarily, we set $k_{nn} = 7$ in the following simulations, inspired by experimental measurements on flocks of starlings [13], in spite of the fact that our system is two-dimensional. So the value of k_{nn} adopted in the present work follows from a compromise: on the one hand, it is not so large as to avoid mean-field-like behavior, and on the other hand, it is not so small as to allow the occurrence of ordered states. Summing up, our choice falls

in an interval such that the number of interacting neighbors is irrelevant for the characterization of the critical behavior.

Let us first discuss stationary measurements. Figure 1(a) shows plots of the order parameter ϕ versus the noise where we can observe the order-disorder transition. The susceptibility $\chi \equiv L^2(\langle \phi^2 \rangle - \langle \phi \rangle^2)$ versus the noise η, shown in Fig. 1(b), gives evidence of the large fluctuations of the order parameter that occur near the phase transition. To verify that the phase transition is second order and to find the critical noise, we compute the dependence on the noise of the fourth-order Binder cumulant, $U \equiv 1 - \frac{\langle \phi^4 \rangle}{3\langle \phi^2 \rangle^2}$. The curves corresponding to different system sizes [Fig. 2(a)] cross each other at the critical point, allowing us to identify the critical noise $\eta_c = 0.039\,75 \pm 0.000\,25$. Figure 2(b) shows the behavior of U in a wider noise interval where no evidence of first-order-like behavior ($U < 0$) is observed. It is worth mentioning that the nature of the order-disorder transition in the metric Vicsek model, i.e., first versus second order, has been treated by many authors [3–6,14,17–19], and a detailed discussion is beyond the scope of this article. Hence, in this paper we observed

FIG. 1. (Color online) Stationary measurements of (a) the order parameter and (b) susceptibility, corresponding to four system sizes.
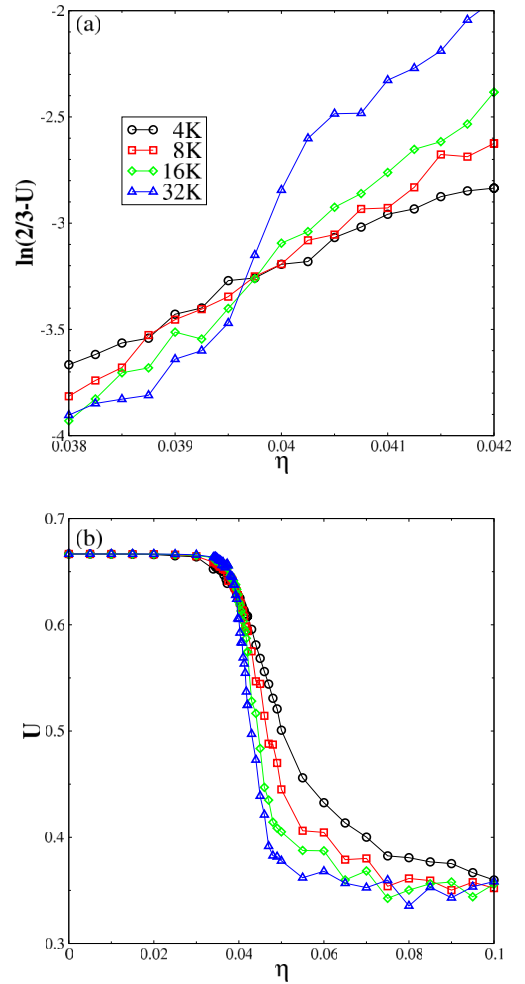
FIG. 2. (Color online) Stationary measurements of the Binder cumulant, corresponding to four system sizes. (a) At the critical noise $\eta_c = 0.039\,75(25)$, the cumulant has the same value for all system sizes. The variable $\ln(2/3 - U)$ was chosen to depict smooth curves. (b) Overview of the Binder cumulant for the whole range of the order-disorder transition.
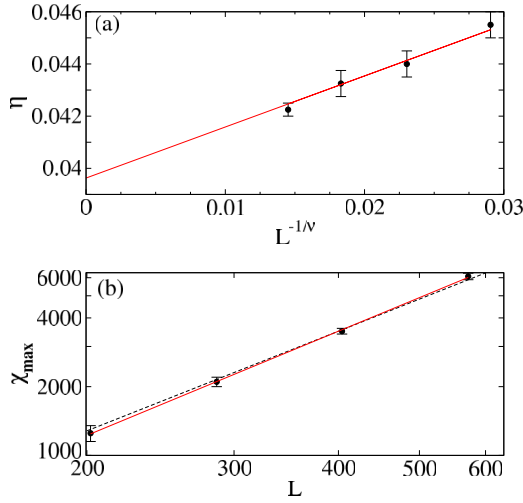
FIG. 3. (Color online) (a) Scaling plot of the peak position of the susceptibility vs system size, according to $\eta_{\max}(L) = \eta_c +$ const$L^{-1/1.34}$. The extrapolation to $L \to \infty$ gives $\eta_c = 0.0397 \pm 0.0001$. (b) Log-log plot of the maximum value of the susceptibility vs $L^{\gamma/\nu}$, which allows us to determine $\gamma/\nu = 1.51(3)$ (solid line). The dashed line corresponds to $\gamma/\nu = 1.45(3)$, which was already reported for the metric model [6].

second-order behavior through Eq. (2) by using a backward update, angular noise, and staying within the low-density and low-velocity regime.

For second-order transitions, it is known that the maximum fluctuation of the order parameter $\chi_{\max}$, which corresponds to

the position of the peaks in Fig. 1(b), is located at L-dependent pseudocritical noises $\eta_{\max}(L)$. The maxima corresponding to different sample sizes scale as $\chi_{\max} \propto L^{\gamma/\nu}$ [Fig. 3(b)], where γ and ν are the susceptibility and correlation length exponents, respectively. The best fit of the data yields $\gamma/\nu = 1.51 \pm 0.03$ (solid line), which is in agreement (within error bars) with the value 1.45(3) (dashed line) already reported for the metric model [6]. Furthermore, the location of those maxima scales as $\eta_{\max}(L) = \eta_c + \text{const} L^{-1/\nu}$, as confirmed in Fig. 3(a). Here, we assume $\nu = 1.34 \pm 0.08$, as determined by means of dynamic measurements (see below), and the best fit of the data allows us to recover $\eta_c = 0.0397 \pm 0.0001$, in excellent agreement with our previous determination employing the cumulant.

On the other hand, dynamic measurements of the topological model are quite demanding and require the simulation of systems of 65 536 agents in order to obtain reliable exponents. By starting the system from a randomly disordered state, one expects that the fluctuations of the order parameter at criticality, during the short-time regime, will increase according to $\chi(t) \propto t^{\frac{\gamma}{\nu z}}$ [20,21]. This result is verified in Fig. 4(a). The best fit of the data yields $\frac{\gamma}{\nu z} = 1.01(5)$.

Relaxation dynamic measurements are performed by quenching the system at the critical point starting from an ordered initial state. Such a state is obtained from the natural time evolution of the system up to the stationary regime at zero noise from a random initial state. Near the critical point of second-order transitions, the time evolution of relevant observables follows scaling laws [20,21]. In fact, the
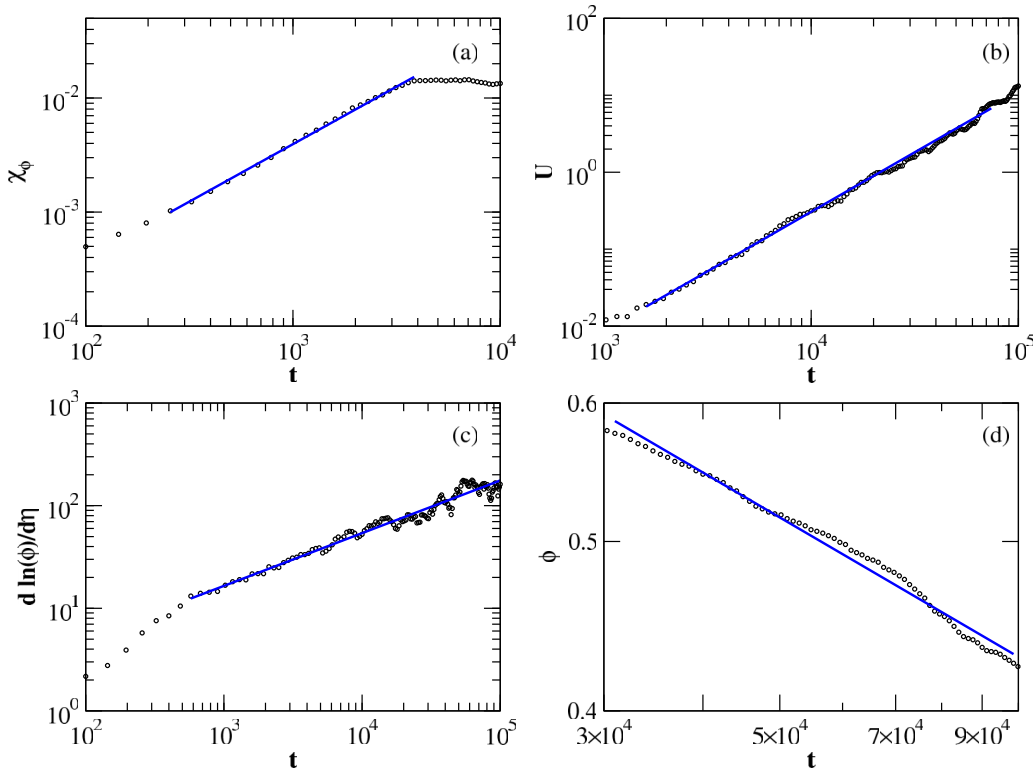
FIG. 4. (Color online) Dynamic measurement for a system of 65 536 agents. (a) The rise in the order of the system from a randomly disordered initial state gives $\gamma/z\nu = 1.008(9)$. (b) The second-order Binder cumulant provides $d/z = 1.55(3)$. (c) The logarithmic derivative of ϕ gives $1/z\nu = 0.58(6)$. (d) The time evolution of the order parameter gives $\beta/z\nu = 0.265(5)$.

TABLE I. Relationships between the exponents measured in this work for topological interactions and previous results corresponding to metric interactions [6] and the critical exponents determined by using those relationships.

	γ/ν	$\beta/z\nu$	d/z	$1/z\nu$	$\gamma/z\nu$
Topological	1.51(3)	0.26(1)	1.55(3)	0.58(6)	1.01(5)
Metric	1.45(3)	0.25(2)	1.57(2)	0.6(1)	1.12(3)
	Critical exponents				
	γ	ν	z	β	
Topological	1.74(20)	1.34(8)	1.29(2)	0.59(7)	
Metric	1.87(4)	1.3(3)	1.27(2)	0.42(4)	

second-order Binder cumulant, $U^*(t) \equiv \frac{\langle\phi^2\rangle - \langle\phi\rangle^2}{\langle\phi\rangle^2}$, would behave as $U^* \propto t^{d/z}$ [Fig. 4(b)], the logarithmic derivative of the order parameter evaluated at criticality would scale as $\frac{\partial \ln \phi}{\partial \tilde{\eta}} \propto t^{1/z\nu}$ [Fig. 4(c)], and the order parameter follows $\phi(t) \propto t^{-\beta/z\nu}$ [Fig. 4(d)]. The best fits of the data yield the following relationships for the critical exponents: $\beta/z\nu = 0.26 \pm 0.01$, $d/z = 1.55 \pm 0.03$, and $1/z\nu = 0.58 \pm 0.06$. Also, the hyperscaling relationship, $d\nu - 2\beta - \gamma = 0$, gives

$$\frac{d}{z} - 2\frac{\beta}{z\nu} - \frac{\gamma}{z\nu} = 0.012(49)$$

and becomes satisfied for dynamic measurements of the topological model.

The complete set of relationships between critical exponents measured in this work and their counterparts obtained for the metric case [6] are summarized in Table I. Also, Table I shows the values of the corresponding critical exponents for both cases.

As an additional test of our results, we perform a finite-size scaling analysis of the raw data corresponding to stationary measurements of the order parameter, the susceptibility, and the cumulant (cf. Fig. 5). In all cases we obtain excellent data collapse, which confirms the validity of the theory and further supports our numerical data.

A careful comparison of both the relationships between exponents and the exponents themselves (see Table I) reveals that most of the magnitudes are very close to each other (within less than 10% of the error bars). Thus this result leads us to conclude that the Vicsek model defines a robust universality class that is independent of the type of interactions used, i.e., topological or metric.

In order to further compare the critical behavior of the topological and metric models we analyzed many configurations of the system close to the critical noise. Figure 6 shows a typical configuration obtained at the steady state of the system with $N = 32\,000$. Since the agents in the system tend to aggregate in clusters of many sizes, we assume that two agents placed at a distance less than an arbitrary cutoff radius belong to the same cluster. Density fluctuations become evident through the onset of an incipient traveling band (on the right-hand side of the figure) due to cluster correlations. Given the cluster size distribution $p(m) = mn_m/N$, where n_m is the number of clusters having m agents, we compute it over 100 different configurations in order to characterize its behavior
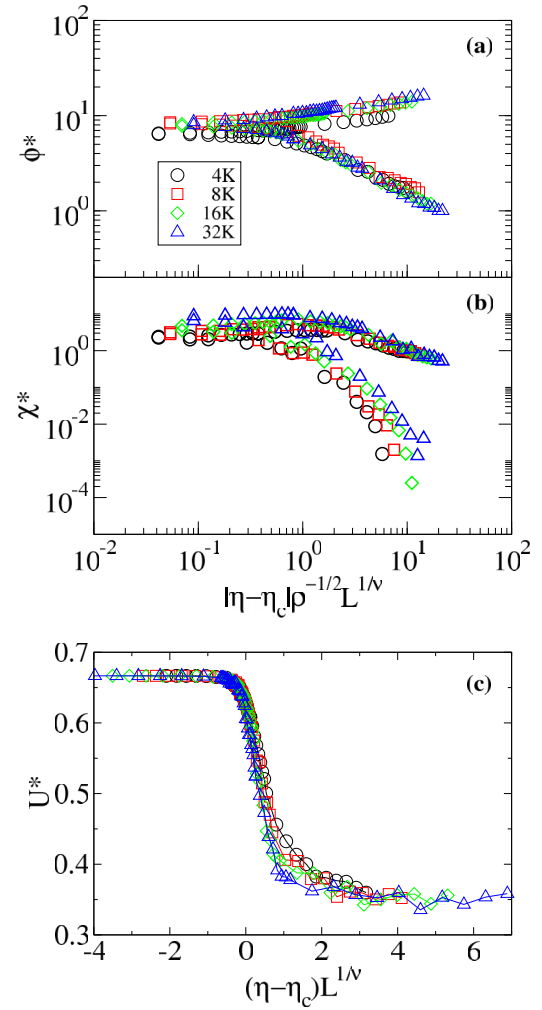
FIG. 5. (Color online) Scaling plots corresponding to the stationary measurements already shown in Figs. 1 and 2. (a) Scaling of the order parameter according to $\phi L^{\beta/\nu}$ vs $(|\eta - \eta_c|L^{1/\nu})/\rho^{1/2}$. (b) Susceptibility, namely, log-log plots of $\chi L^{\gamma/\nu}$ vs $(|\eta - \eta_c|L^{1/\nu})/\rho^{1/2}$. (c) Binder cumulant versus $(\eta - \eta_c)L^{1/\nu}$.

at the critical point. The resulting distribution, and especially its tail (Fig. 7), resembles the one recently reported for the metric model [22]. The existence of a maximum near $m = 25$ is due to the *metric* nature of the definition adopted to compute clusters. In this way, one leaves alone several agents that are far away from any cluster, despite the fact that they interact topologically with some agents. These agents represent less than 0.5% of the whole system and become irrelevant over the statistic weight of the distribution tail. In order to compare the distribution obtained with results corresponding to the metric model, we performed a power-law fitting of the form $p(m) \propto m^{-\zeta}$ along the tail of this distribution, and the exponent obtained is $\zeta = 1.3 \pm 0.1$. This figure is indistinguishable from equivalent exponents reported in simulations of the metric model [23,24], experimental results [7,25], and kinetic modeling [22].

It is worth mentioning that second-order behavior has also been reported in another topological model [14]. However, that model is basically different from the one proposed here since
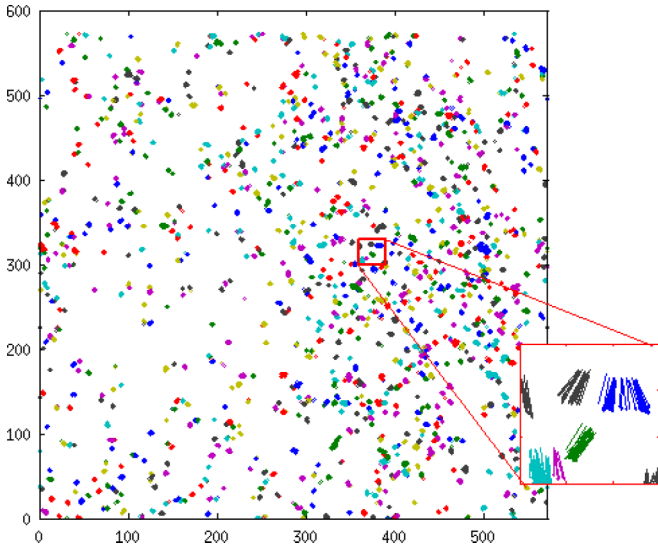
FIG. 6. (Color online) Snapshot of a typical configuration close to the critical point for $N = 32\,000$. An incipient traveling band (right-hand side) is formed by correlated clusters. Agents belonging to the same cluster are labeled with the same color.

vectorial noise is assumed and the neighbors are chosen by means of Voronoi tessellation [14]. Therefore some reported critical exponents are different from those presented here. One reason for this discrepancy becomes evident from Fig. 6: evaluation of Voronoi neighboring implies that all agents must have neighborgs in all directions, hence, due to periodic boundary conditions, percolation among the conected agents can be present in all directions avoiding the cluster formation. Such effect is not observed in the model proposed here. In fact, in our model with fixed neighbors, an agent could have all its k_{nn} neighbors along a given direction. At the critical point, percolation clusters are those whose correlations allow the formation of traveling waves across the space, such as the one observed in Fig. 6, as was pointed out in [22]. Summing up, it is not surprising that a model with Voronoi neighboring and vectorial noise might belong to a different universality class than that of both the standard Vicsek model and the topological model proposed in this paper.
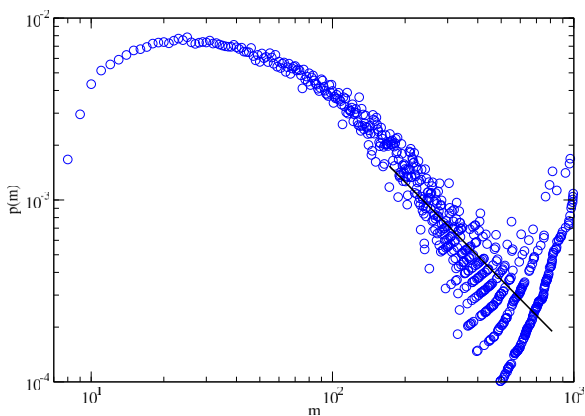
FIG. 7. (Color online) Cluster size distribution $p(m)$ vs the cluster size m. A power-law fitting (solid line) gives the exponent $\zeta = 1.3(1)$.
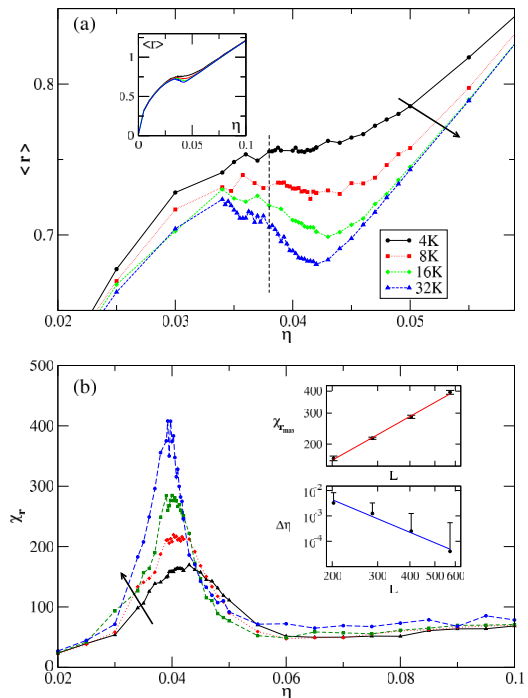
FIG. 8. (Color online) (a) Mean radius $\langle r \rangle$ required by an agent for a topological interaction with seven neighbors near the critical point $\eta_c = 0.039\,75$. Note that $\langle r \rangle$ has a maximum and a minimum located on both sides of the critical noise (vertical dashed line), which are more pronounced for larger system sizes, as indicated by the arrow. The inset shows the dependence of $\langle r \rangle$ on the noise for the whole domain explored. (b) Plots of the fluctuations of $\langle r \rangle$ vs the noise. The top and bottom insets show the scaling behavior of the maximum fluctuation and its position, respectively. Further details are given in the text.

Very interesting features of the topological model arise when assessing the average radius $\langle r \rangle$ that each agent needs in order to just interact with seven neighbors. In fact, the inset of Fig. 8(a) shows plots of $\langle r \rangle$ versus the noise obtained for systems of different size. As is expected from a topological model, far from criticality the averaged radius is independent of the system size. However, close enough to the critical point, it is found that the curves develop both a local maximum and a local minimum, depending on the system size. Furthermore, they exhibit the inflexion point very close to the critical noise. At criticality, the agents require an average radius smaller than unity, i.e., the radius used in the case of the metric Vicsek model, in order to locate their seven partners. In fact, in the density and velocity regimes studied, over 20 neighbors can typically be found inside a unitary radius. On the other hand, Fig. 8(b) shows the noise dependence of the fluctuations of the average radius defined as $\chi_r = (\langle r^2 \rangle - \langle r \rangle^2)L^2$. It follows that χ_r exhibits a sharp peak at the critical noise. Indeed, the location of the maximum scales as $\Delta\eta = \eta - \eta_c \propto L^{-4.3(4)}$. Furthermore, the peak height scales as $\chi_{r_{\max}} \propto L^{0.83(3)}$. The fittings performed in order to obtain the scaling relationships are depicted in the corresponding insets of Fig. 8(b). Thus, at the critical noise, the mean area that an agent has to scan in order to find seven neighbors undergoes large fluctuations that diverge with the system size.

Cavagna *et al.* [26] have stated that a real flock remains at the edge of criticality, i.e., in a state close enough to the critical point to get the maximum adaptability without losing its cohesion. Hence, let us consider any flock (natural, artificial, or theoretical) whose agents attempt to stand at the highest possible value of the noise but inside the ordered state in order to get the maximum response without loss of cohesion. How could they achieve such a state? The results summarized in Fig. 8 allow us to conjecture a simple mechanism to answer that question: as the noise rises, the average spatial range required for each agent to establish interactions with a prefixed number of partners starts to undergo large fluctuations, as shown in Fig. 8(b). These fluctuations would perturb the agents, e.g., by demanding a large effort in order to locate their neighboring partners, so each agent should be able to realize that it is time to change its moving strategy. Of course, individuals in larger flocks have a better chance to note such fluctuations. Furthermore, Fig. 8(a) could provide a clue about a competing mechanism that would prevent the formation of very large flocks: the occurrence of well-defined local maxima and minima in the average radius of interaction close to critically implies that the optimum radius of interaction of each agent occurs at three different values of noise, and at least one of them is always in the disordered phase. Hence, an iterative process that discards agents that fail to detect both situations is a suitable candidate for the development of an optimization mechanism capable of describing how a system of interacting self-propelled particles can evolve in order to find their optimum size. If this mechanism were natural selection, flocks would have to evolve into typical

sizes that place them in the best situation. Also, by adopting the above-discussed mechanisms, artificial swarms of microrobots can be designed to fit sizes that allow cohesion without the need for external orders.

IV. CONCLUDING REMARKS

We have shown that both a topological model with a fixed number of neighbors and the metric Vicsek model belong to the same universality class, which in turn seems to be quite robust. Furthermore, the cluster size distribution evaluated at the critical point follows a power-law behavior with the same exponent as in the metric case, which is another feature shared by both systems. It is known that many systems in nature exhibit critical behavior [27,28], and such a state can be related to optimization, as we have conjectured. The measurement of the mean radius of interaction and its fluctuations, as discussed here, may provide an original way to get insight into this challenging topic in both theoretical and experimental biology. While the outlined arguments are rather speculative and more biological evidence must be gathered to support it, our results provide a mechanism to design and control artificial swarms in both robotics and drug delivery.

[1] T. Vicsek, A. Czirók, E. Ben-Jacob, I. Cohen, and O. Shochet, Phys. Rev. Lett. **75**, 1226 (1995).

[2] E. V. Albano, Phys. Rev. Lett. **77**, 2129 (1996).

[3] G. Grégoire and H. Chaté, Phys. Rev. Lett. **92**, 025702 (2004).

[4] M. Aldana, H. Larralde, and B. Vázquez, J. Mod. Phys. B **23**, 3661 (2009).

[5] T. Vicsek and A. Zafeiris, Phys. Rep. **517**, 71 (2012).

[6] G. Baglietto and E. V. Albano, Phys. Rev. E **80**, 050103 (2009).

[7] F. Peruani, J. Starruss, V. Jakovljevic, L. Sogaard-Andersen, A. Deutsch, and M. Bär, Phys. Rev. Lett. **108**, 098102 (2012).

[8] V. Schaller and A. R. Bausch, Proc. Natl. Acad. Sci. USA **110**, 4488 (2013).

[9] L. Coburn, L. Cerone, C. Torney, I. D. Couzin, and Z. Neufeld, Phys. Biol. **10**, 046002 (2013).

[10] D. H. Kelley and N. T. Ouellette, Sci. Rep. **3**, 1073 (2013).

[11] W. Bialek, A. Cavagna, I. Giardina, T. Mora, and E. Silvestri, Proc. Natl. Acad. Sci. USA **109**, 4786 (2012).

[12] A. Cavagna, A. Cimarelli, I. Giardina, A. Orlandi, G. Parisi, A. Procaccini, R. Santagati, and F. Stefanini, Math. Biosci. **214**, 32 (2008).

[13] M. Ballerini, N. Cabibbo, R. Candelier, A. Cavagna, E. Cisbani, I. Giardina, V. Lecomte, A. Orlandi, G. Parisi, A. Procaccini *et al.*, Proc. Natl. Acad. Sci. USA **105**, 1232 (2008).

[14] F. Ginelli and H. Chaté, Phys. Rev. Lett. **105**, 168103 (2010).

[15] J. Gautrais, F. Ginelli, R. Fournier, S. Blanco, M. Soria, H. Chaté, and G. Theraulaz, PLoS Comput. Biol. **8**, e1002678 (2012).

[16] A. Peshkov, S. Ngo, E. Bertin, H. Chaté, and F. Ginelli, Phys. Rev. Lett. **109**, 098101 (2012).

[17] G. Baglietto and E. V. Albano, Phys. Rev. E **78**, 021125 (2008).

[18] M. Aldana, V. Dossetti, C. Huepe, V. M. Kenkre, and H. Larralde, Phys. Rev. Lett. **98**, 095702 (2007).

[19] M. Nagy, I. Daruka, and T. Vicsek, Phys. A **373**, 445 (2007).

[20] H. Janssen, B. Schaub, and B. Schmittmann, Z. Phys. B **73**, 539 (1989).

[21] E. V. Albano and G. Saracco, Phys. Rev. Lett. **88**, 145701 (2002).

[22] F. Peruani and M. Bär, New J. Phys. **15**, 065009 (2013).

[23] Y. Yang, V. Marceau, and G. Gompper, Phys. Rev. E **82**, 031904 (2010).

[24] F. Peruani, A. Deutsch, and M. Bär, Phys. Rev. E **74**, 030904(R) (2006).

[25] H. Zhang, A. Be'er, E. Florin, and H. Swinney, Proc. Natl. Acad. Sci. USA **107**, 13526 (2010).

[26] A. Cavagna, A. Cimarelli, I. Giardina, G. Parisi, R. Santagati, F. Stefanini, and M. Viale, Proc. Natl. Acad. Sci. USA **107**, 11865 (2010).

[27] H. J. Jensen, *Self-Organized Criticality: Emergent Complex Behavior in Physical and Biological Systems* (Cambridge University Press, Cambridge, 1998).

[28] S. Camazine, *Self-Organization in Biological Systems* (Princeton University Press, Princeton, NJ, 2003).